

Information-entropic measures in confined isotropic harmonic oscillator

Neetik Mukherjee* and Amlan K. Roy†

Department of Chemical Sciences

Indian Institute of Science Education and Research (IISER) Kolkata,

Mohanpur-741246, Nadia, WB, India

Abstract

Information based uncertainty measures like Rényi entropy (R), Shannon entropy (S) and Onicescu energy (E) (in both position and momentum space) are employed to understand the influence of radial confinement in isotropic harmonic oscillator. The transformation of Hamiltonian in to a dimensionless form gives an idea of the composite effect of oscillation frequency (ω) and confinement radius (r_c). For a given quantum state, accurate results are provided by applying respective *exact* analytical wave function in r space. The p -space wave functions are produced from Fourier transforms of radial functions. Pilot calculations are done taking order of entropic moments (α, β) as $(\frac{3}{5}, 3)$ in r and p spaces. A detailed, systematic analysis is performed for confined harmonic oscillator (CHO) with respect to state indices n_r, l , and r_c . It has been found that, CHO acts as a bridge between particle in a spherical box (PISB) and free isotropic harmonic oscillator (IHO). At smaller r_c , E_r increases and R_r^α, S_r decrease with rise of n_r . At moderate r_c , there exists an interaction between two competing factors: (i) radial confinement (localization) and (ii) accumulation of radial nodes with growth of n_r (delocalization). Most of these results are reported here for the first time, revealing many new interesting features.

PACS: 03.65-w, 03.65Ca, 03.65Ta, 03.65.Ge, 03.67-a.

Keywords: Rényi entropy, Shannon entropy, Onicescu energy, Confined isotropic harmonic oscillator, Particle in a symmetric box.

*Email: neetik.mukherjee@iiserkol.ac.in.

†Corresponding author. Email: akroy@iiserkol.ac.in, akroy6k@gmail.com.

I. INTRODUCTION

In recent years, interest in studying spacially confined quantum systems has enhanced significantly. A quantum mechanical particle under extreme pressure environment exhibits many fascinating, notable physical and chemical properties [1–3]. Discovery and development of modern experimental techniques have also inspired extensive research activity to explore and study such systems [2–7]. They have potential applications in a wide range of problems namely, quantum wells, quantum wires, quantum dots, defects in solids, superlattice structure, as well as nano-sized circuits such as quantum computer, etc. Besides, they have uses in cell-model of liquid, high-pressure physics, astrophysics [8], study of impurities in semiconductor materials, matrix isolated molecules, endohedral complexes of fullerenes, zeolites cages, helium droplets, nano-bubbles, [2] etc.

In last ten years, extensive theoretical works have been published covering a wide variety of confining potentials. Two such prototypical systems that have received maximum attention are confined harmonic oscillator (CHO) (in 1D, 2D, 3D, and D dimension) [9–11, 13–15] and confined hydrogen atom (CHA) inside a spherical enclosure [3, 10, 16–25]. The (CHO) model within an impenetrable barrier was explored quite extensively leading to a host of interesting properties—both from physical and mathematical perspective. They offer some unique phenomena, especially relating to *simultaneous, incidental and inter-dimensional* degeneracy [15]. A large variety of theoretical methods were employed; a selected set includes perturbation theory, Padé approximation, WKB method, Hypervirial theorem, power-series solution, super-symmetric quantum mechanics, Lie algebra, Lagrange-mesh method, asymptotic iteration method, generalized pseudo-spectral method, etc. [16–24] and references therein. *Exact* solutions [20] are expressible in terms of Kummer confluent hypergeometric function.

In recent years, significant attention was paid to explore various information measures (IE), namely, Fisher information (I), Shannon entropy (S), Rényi entropy (R), Onicescu energy (E) and several complexities in a multitude of physical, chemical systems, including central potentials. The literature is quite vast. In a quantum system, R, called information generating functionals, is closely related to entropic moments (discussed later), and completely characterize density $\rho(\mathbf{r})$. It is successfully used to investigate and predict certain quantum properties and phenomena like entanglement, communication protocol, correlation

de-coherence, measurement, localization properties of Rydberg states, molecular reactivity, multi-fractal thermodynamics, production of multi-particle in high-energy collision, disordered systems, spin system, quantum-classical correspondence, localization in phase space [34–40], etc. It is interesting to note that, S , E are two particular cases of R [41, 42]. S and E quantify the information content in different and complimentary way. Former refers to the expectation value of logarithmic probability density function and is a global measure of spread of density. On the other hand, E is quantified as the second-order entropic moment [43]. It becomes minimum for equilibrium and hence often termed as disequilibrium. In recent years, S is examined in a number of systems, such as, Pöschl-Teller [44], Rosen-Morse [45], pseudo-harmonic [46], squared tangent well [47], hyperbolic [48], position-dependent mass Schrödinger equation [49, 50], infinite circular well [51], hyperbolic double-well (DW) potential [52], etc. Recently, some of these measures have been found to be quite efficient and useful to explain the oscillation and localization-delocalization behavior of a particle in symmetric and asymmetric DW potential [53, 54], as well as in a confined 1D quantum harmonic oscillator [14].

IE quantifies the spatial delocalization of single-particle density of a system in several complimentary ways. Arguably, these are the most appropriate uncertainty measures, as they do not make any reference to some specific point of the resembling Hilbert space. Moreover, these are closely related to some energetic and experimentally measurable quantities [41, 55] of a system. In case of R and S , some lower bound is available, which do not depend on quantum number. But, for I both upper and lower bounds have been established, which strictly change with quantum numbers [42, 56, 57].

A vast majority of IE-related works, mentioned above and elsewhere, deal with a *free or unconfined* systems. However, such study for *confined* quantum systems is very rare. In last few years, some such results have been published for symmetric and asymmetrically confined 1-D harmonic oscillator [14, 26] and confined hydrogen atom [27–30]. However, to the best of our knowledge, such investigation for a 3-D CHO system has not yet been done. Hence, it would be highly desirable to explore and inspect these quantities for such system in some detail. In this work, we have pursued a detailed analysis of R , S , E for CHO. Moreover, we have transformed our original Hamiltonian into a dimensionless form [31] to make the results more general and interesting, from the view point of an experimentalists [32, 33]. This modification leads to a dimensionless parameter $\left(\eta = \frac{m\omega r_c^4}{\hbar^2}\right)$, which depends

on the product of ω and quartic power of r_c . Thus, at first, we analyze the variation of R, S, E for an arbitrary state in CHO for small, intermediate and large regions of η in conjugate r , p spaces. Later, we proceed for a detailed exploration of these measures as functions of r_c . These are provided for a general state having principal and azimuthal quantum numbers n , l , while keeping magnetic quantum number $m = 0$. In r space all the calculations are performed taking exact wave function. However, such expressions are unavailable in p -space, and hence numerical Fourier transforms require to be carried out. It is important to note that, no such literature is available for CHO. This work has been arranged in the following manner. Section 2, gives the essential points of methodology, then Section 3 provides a details discussion on the results of aforesaid measures for CHO, while we conclude with a few remarks in section 4.

II. METHODOLOGY

The time-independent, non-relativistic wave function for a CHO system, in r space may be expressed as,

$$\Psi_{n_r,l,m}(\mathbf{r}) = \psi_{n_r,l}(r) Y_{l,m}(\Omega), \quad (1)$$

with r and Ω illustrating the radial distance and solid angle successively. Here $\psi_{n,l}(r)$ represents the radial part and $Y_{l,m}(\Omega)$ identifies spherical harmonics. The pertinent radial Schrödinger equation under the influence of confinement is (atomic unit employed unless mentioned otherwise),

$$\left[-\frac{1}{2} \frac{d^2}{dr^2} + \frac{l(l+1)}{2r^2} + v(r) + v_c(r) \right] \psi_{n_r,l}(r) = \mathcal{E}_{n_r,l} \psi_{n_r,l}(r), \quad (2)$$

where $v(r) = \frac{1}{2}\omega^2 r^2$. Our required confinement effect is introduced by invoking the following potential: $v_c(r) = +\infty$ for $r > r_c$, and 0 for $r \leq r_c$, where r_c signifies radius of confinement.

Exact generalized radial wave function for a CHO is mathematically expressed as [15],

$$\psi_{n_r,l}(r) = N_{n_r,l} r^l {}_1F_1 \left[\frac{1}{2} \left(l + \frac{3}{2} - \frac{\mathcal{E}_{n_r,l}}{\omega} \right), \left(l + \frac{3}{2} \right), \omega r^2 \right] e^{-\frac{\omega}{2} r^2}. \quad (3)$$

Here, $N_{n_r,l}$ represents normalization constant and $\mathcal{E}_{n_r,l}$ corresponds to the energy of a given state characterized by quantum numbers n_r, l , whereas ${}_1F_1[a, b, r]$ signifies confluent hypergeometric function. Allowed energies are computed by applying the boundary condition $\psi_{n_r,l}(0) = \psi_{n_r,l}(r_c) = 0$. In this work, generalized pseudospectral (GPS) method was used

to evaluate $\mathcal{E}_{n_r,l}$ of these states. This method has provided highly accurate results for various model and real systems including atoms, molecules, some of which could be found in the references [24, 58, 60?]. This is very well documented and therefore omitted here.

The p -space wave function is obtained from Fourier transform of r -space counterpart,

$$\begin{aligned}\psi_{n_r,l}(p) &= \frac{1}{(2\pi)^{\frac{3}{2}}} \int_0^{r_c} \int_0^\pi \int_0^{2\pi} \psi_{n_r,l}(r) \Theta(\theta) \Phi(\phi) e^{ipr \cos \theta} r^2 \sin \theta \, dr d\theta d\phi \\ &= \frac{1}{2\pi} \sqrt{\frac{2l+1}{2}} \int_0^{r_c} \int_0^\pi \psi_{n_r,l}(r) P_l^0(\cos \theta) e^{ipr \cos \theta} r^2 \sin \theta \, dr d\theta.\end{aligned}\quad (4)$$

Here $\psi_{n_r,l}(p)$ is not normalized and needs to be normalized. Integrating over θ and ϕ yields,

$$\psi_{n_r,l}(p) = (-i)^l \int_0^{r_c} \frac{\psi_{n_r,l}(r)}{p} f(r, p) dr, \quad (5)$$

where, $f(r, p)$ depends only on l quantum number. It can be expressed in terms of *Cosine* and *Sine* series. More details about $f(r, p)$ could be found in [27].

Rényi entropies of order $\lambda (\neq 1)$ are obtained by taking logarithm of λ -order entropic moment. In spherical polar coordinate these can be written as,

$$\begin{aligned}R_{\mathbf{r}}^\lambda &= \frac{1}{(1-\lambda)} (\ln 2\pi + \ln[\omega_r^\lambda] + \ln[\omega_{(\theta,\phi)}^\lambda]) , \\ R_{\mathbf{p}}^\lambda &= \frac{1}{(1-\lambda)} (\ln 2\pi + \ln[\omega_p^\lambda] + \ln[\omega_{(\theta,\phi)}^\lambda]) .\end{aligned}\quad (6)$$

Here ω_τ^λ s are entropic moments in τ (r or p or θ) space with order λ , having forms,

$$\omega_r^\lambda = \int_0^\infty [\rho(r)]^\lambda r^2 dr, \quad \omega_p^\lambda = \int_0^\infty [\Pi(p)]^\lambda p^2 dp, \quad \omega_{(\theta,\phi)}^\lambda = \int_0^\pi [\chi(\theta)]^\lambda \sin \theta d\theta. \quad (7)$$

If λ corresponds to α, β in r, p spaces respectively, then for \mathbf{R} , they obey the condition $\frac{1}{\alpha} + \frac{1}{\beta} = 2$. Then one can define total Rényi entropy as $R_t^{(\alpha,\beta)}$ [41, 42], satisfying the following bounds,

$$\begin{aligned}R_t^{(\alpha,\beta)} &= \frac{2-\alpha-\beta}{(1-\alpha)(1-\beta)} \ln 2\pi + \frac{1}{(1-\alpha)} (\ln[\omega_r^\alpha] + \ln[\omega_{(\theta,\phi)}^\alpha]) + \frac{1}{(1-\beta)} (\ln[\omega_p^\beta] + \ln[\omega_{(\theta,\phi)}^\beta]) \\ &\geq 3 \times \left[-\frac{1}{2} \left(\frac{1}{1-\alpha} \ln \frac{\alpha}{\pi} + \frac{1}{1-\beta} \ln \frac{\beta}{\pi} \right) \right].\end{aligned}\quad (8)$$

$S_{\mathbf{r}}, S_{\mathbf{p}}$ and total Shannon entropy S_t are expressed in terms of expectation values of logarithmic probability density functions, which for a central potential further simplifies

TABLE I: $R_{\mathbf{r}}^\alpha, R_{\mathbf{p}}^\beta, R_t^{(\alpha,\beta)}$ for $1s, 1p, 1d$ states in PISB and CHO (six selected η). See text for detail.

State	Property	PISB($\eta = 0$)	$\eta = 0.0001$	$\eta = 0.0625$	$\eta = 1.0$	$\eta = 5.0625$	$\eta = 45.6976$	$\eta = 104.8576$
1s	$R_{\mathbf{r}}^\alpha$	0.871064	0.87106349	0.87060118	0.86363060	0.83292175	0.50791919	0.09617311
	$R_{\mathbf{p}}^\beta$	5.3391	5.339416	5.339830	5.346081	5.373798	5.678841	6.080846
	$R_t^{(\alpha,\beta)}$	6.2101	6.210480	6.210431	6.209712	6.206720	6.186760	6.177019
1p	$R_{\mathbf{r}}^\alpha$	0.740619	0.74061892	0.74041416	0.73732009	0.72353315	0.55729149	0.27721065
	$R_{\mathbf{p}}^\beta$	5.8987	5.898746	5.898972	5.902381	5.917583	6.101146	6.406884
	$R_t^{(\alpha,\beta)}$	6.6393	6.639365	6.639386	6.639701	6.641116	6.658438	6.684095
1d	$R_{\mathbf{r}}^\alpha$	0.789638	0.78963611	0.78953691	0.78803644	0.78131257	0.69457347	0.51883620
	$R_{\mathbf{p}}^\beta$	6.3210	6.321199	6.321338	6.323450	6.332867	6.449503	6.670819
	$R_t^{(\alpha,\beta)}$	7.1106	7.110835	7.110875	7.111487	7.114179	7.144076	7.189655

[56] as below,

$$\begin{aligned}
S_{\mathbf{r}} &= - \int_{\mathcal{R}^3} \rho(\mathbf{r}) \ln[\rho(\mathbf{r})] d\mathbf{r} = 2\pi (S_r + S_{(\theta,\phi)}), \\
S_{\mathbf{p}} &= - \int_{\mathcal{R}^3} \Pi(\mathbf{p}) \ln[\Pi(\mathbf{p})] d\mathbf{p} = 2\pi (S_p + S_{(\theta,\phi)}), \\
S_t &= 2\pi [S_r + S_p + 2S_{(\theta,\phi)}] \geq 3(1 + \ln \pi),
\end{aligned} \tag{9}$$

where the quantities S_r, S_p and S_θ are defined as [56],

$$\begin{aligned}
S_r &= - \int_0^\infty \rho(r) \ln[\rho(r)] r^2 dr, & S_p &= - \int_0^\infty \Pi(p) \ln[\Pi(p)] p^2 dp, \\
\rho(r) &= |\psi_{n,l}(r)|^2, & \Pi(p) &= |\psi_{n,l}(p)|^2, \\
S_{(\theta,\phi)} &= - \int_0^\pi \chi(\theta) \ln[\chi(\theta)] \sin \theta d\theta, & \chi(\theta) &= |\Theta(\theta)|^2.
\end{aligned} \tag{10}$$

By definition, E represents the 2nd order entropic moment [41]; therefore choice of $\alpha = \beta = 2$ transforms Eq. (8) into the following form,

$$E_r = \int_0^\infty [\rho(r)]^2 r^2 dr, \quad E_p = \int_0^\infty [\Pi(p)]^2 p^2 dp, \quad E_{\theta,\phi} = \int_0^\pi [\chi(\theta)]^2 \sin \theta d\theta, \quad E = E_r E_p E_{\theta,\phi}^2. \tag{11}$$

where, E_t is the total Onicescu energy. Note that, the restriction $\frac{1}{\alpha} + \frac{1}{\beta} = 2$ holds for R only, and not on E. Hence in our study of R, $\alpha = \frac{3}{5}$ and $\beta = 3$ have been chosen.

III. RESULT AND DISCUSSION

At the beginning, it may be convenient to point out a few things about the presented results. The net information measures in conjugate r and p spaces may be divided into

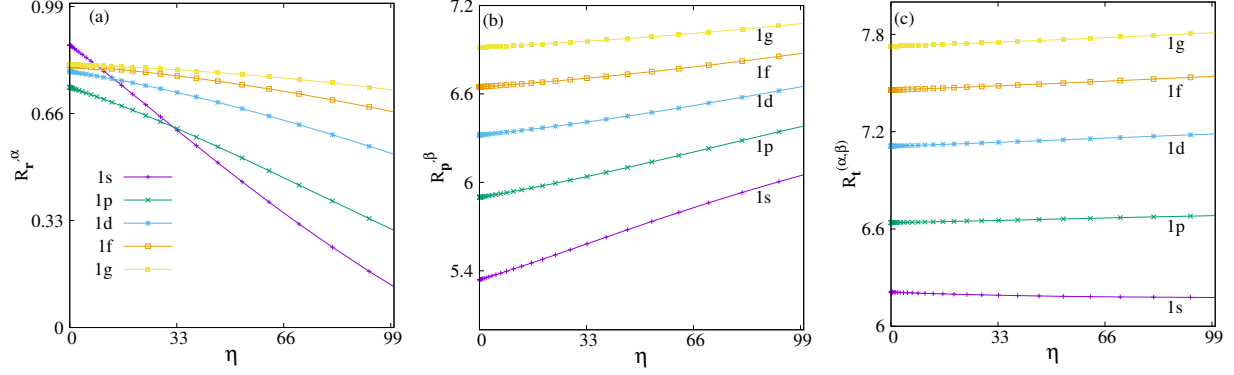


FIG. 1: Plots of R_r^α , R_p^β , $R_t^{(\alpha,\beta)}$ against η for first five circular states of CHO in panels (a), (b), (c) respectively. See text for details.

radial and angular segments. In a given space, the results provided here correspond to net measures including the angular contributions. One can transform the IHO to a CHO by pressing the radial boundary of former from infinity to a finite region. This change in radial environment does not affect the angular boundary conditions. Hence, angular portion of these measures remains invariant in r , p spaces. Furthermore, they change with l , m quantum numbers. Throughout the whole article the magnetic quantum number m is set to 0, unless stated otherwise. Since the wave function, energy and position expectation values of CHO were presented earlier in some details, we do not discuss them in this work. Our primary focus is on information analysis.

Equation (2) may be represented in the following form,

$$\left[-\frac{1}{2} \frac{d^2}{dr^2} + \frac{l(l+1)}{2r^2} + \frac{1}{2} \omega r^2 + V \Theta(r - r_c) \right] \psi_{n,l}(r) = \mathcal{E}_{n,l} \psi_{n,l}(r), \quad (12)$$

$$\Theta(r - r_c) = 0, \text{ at } r \leq |r_c|, \quad \Theta(r - r_c) = 1, \text{ at } r > |r_c|.$$

Here, $\Theta(r - r_c)$ is a Heaviside Theta function and V is a constant, having very large value. The effect of localization and delocalization depends on r_c and ω . It has been observed that, the Hamiltonian can be generalized into a dimensionless form, so that one can correlate experimental observations with theoretical results [31–33]. Further, in 1D case, it is established that ω is proportional to the square root of the magnetic field parallel to the gradient of the confining potential [32]. Hence, it seems appropriate to study composite effect r_c and ω with the aid of a single dimensionless parameter η . This will make our present

TABLE II: $S_{\mathbf{r}'}, S_{\mathbf{p}'}, S_t$ for $1s, 1p, 1d$ states in PISB and CHO (six selected η). See text for detail.

state	Property	PISB($\eta = 0$)	$\eta = 0.0001$	$\eta = 0.0625$	$\eta = 1.0$	$\eta = 5.0625$	$\eta = 45.6976$	$\eta = 104.8576$
1s	$S_{\mathbf{r}'}$	0.675583	0.67558205	0.67493721	0.66522220	0.62260461	0.19387157	-0.28934719
	$S_{\mathbf{p}'}$	5.9416	5.941691	5.941941	5.945800	5.964491	6.266362	6.725853
	S_t	6.6172	6.617273	6.616878	6.611022	6.587096	6.460233	6.436505
1p	$S_{\mathbf{r}'}$	0.520372	0.52037321	0.52010134	0.51599338	0.49769459	0.28018517	-0.06370302
	$S_{\mathbf{p}'}$	6.5098	6.509889	6.509982	6.511416	6.518562	6.670296	7.018161
	S_t	7.0302	7.030263	7.030083	7.027410	7.016257	6.950482	6.954458
1d	$S_{\mathbf{r}'}$	0.552449	0.55244843	0.55231997	0.55037642	0.54166146	0.42931507	0.20823953
	$S_{\mathbf{p}'}$	7.0957	7.095786	7.095821	7.096367	7.099323	7.176126	7.415409
	S_t	7.6482	7.648235	7.648141	7.646743	7.640984	7.605441	7.623648

study more interesting and appropriate from an experimental view point. It follows that,

$$\mathcal{E}_{n_r,l} = \mathcal{E}_{n_r,l} \left(\frac{\hbar^2}{m}, \omega, r_c \right); \quad \psi_{n_r,l} = \psi_{n_r,l} \left(\frac{\hbar^2}{m}, \omega, r_c, r \right). \quad (13)$$

After substitution of $r = r_c r'$ into Eq. (12), the modified dimensionless Schrödinger equation can be written as

$$\left[-\frac{1}{2} \frac{d^2}{dr'^2} + \frac{l(l+1)}{2r'^2} + \frac{1}{2} \eta r'^2 + V\theta(r' - 1) \right] \psi_{n_r,l}(r') = \frac{mr_c^2}{\hbar^2} \mathcal{E}_{n_r,l} \psi_{n_r,l}(r'), \quad (14)$$

Where r' is a dimensionless variable and $\eta = \frac{m\omega r_c^4}{\hbar^2}$. At $\eta = 0$ this represents the PISB Hamiltonian. The above conversion leads to,

$$\begin{aligned} \mathcal{E}_{n_r,l} \left(\frac{\hbar^2}{m}, \omega, r_c \right) &= \frac{\hbar^2}{mr_c^2} \mathcal{E}_{n_r,l} (1, \eta, 1), \\ \psi_{n_r,l} \left(\frac{\hbar^2}{m}, \omega, r_c, r \right) &= \psi_{n_r,l} (1, \eta, 1, r'). \end{aligned} \quad (15)$$

Equation (15) indicates that η depends on the product of ω, m and quartic power of r_c . However, if we choose $m = \hbar = 1$, then the effective dependence remains on the product of r_c^4 and ω .

Third column of Table I at first portrays $R_{\mathbf{r}'}^\alpha, R_{\mathbf{p}'}^\beta$ and $R_t^{(\alpha,\beta)}$ for $1s, 1p, 1d$ orbitals in PISB. Similarly, 4th-9th columns of this table imprints the same for $1s, 1p, 1d$ states in CHO at six selected η values namely 0.0001, 0.0625, 1, 5.0625, 45.6976, 104.8576. These results clearly indicate that, in CHO $R_{\mathbf{r}'}^\alpha$ decreases and $R_{\mathbf{p}'}^\beta$ increases with rise in η . In case of $1s$ state $R_t^{(\alpha,\beta)}$ lowers with η . On the contrary, for $1p, 1d$ states it progresses with elevation of η . Now, it is important to illustrate the behaviour R in CHO at $\eta \rightarrow 0$ region. A careful examination reveals that, in the neighbourhood of $\eta < 1$, CHO has R values comparable with PISB. This

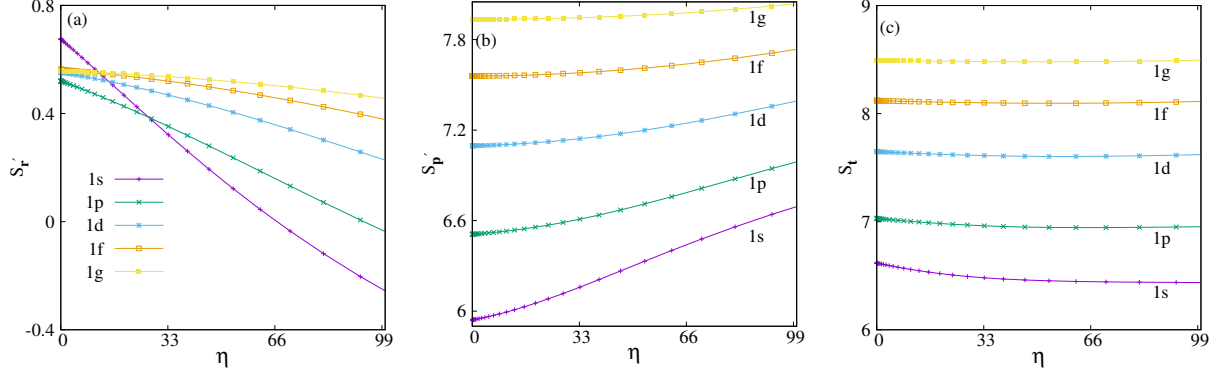


FIG. 2: Plots of $S_{r'}$, $S_{p'}$, S_t against η for first five circular states of CHO in panels (a), (b), (c) respectively. See text for details.

TABLE III: $E_{r'}$, $E_{p'}$, E_t for $1s$, $1p$, $1d$ states in PISB and CHO (six selected η). See text for detail.

state	Property	PISB($\eta = 0$)	$\eta = 0.0001$	$\eta = 0.0625$	$\eta = 1.0$	$\eta = 5.0625$	$\eta = 45.6976$	$\eta = 104.8576$
1s	$E_{r'}$	0.672078	0.6720791	0.67267502	0.68180978	0.72295672	1.23933182	2.09908616
	$E_{p'}$	0.003982	0.003982	0.003982	0.003960	0.003852	0.002818	0.001860
	E_t	0.002678	0.002679	0.002680	0.002700	0.002785	0.003492	0.003904
1p	$E_{r'}$	0.803227	0.80322700	0.80351307	0.80784686	0.82740709	1.09024283	1.62179448
	$E_{p'}$	0.002277	0.002277	0.002277	0.002269	0.002236	0.001858	0.001354
	E_t	0.001829	0.001829	0.001829	0.001833	0.001850	0.002026	0.002197
1d	$E_{r'}$	0.851258	0.85125726	0.85139660	0.85350774	0.86304220	0.99491879	1.297877781
	$E_{p'}$	0.001378	0.001377	0.001377	0.001375	0.001363	0.001214	0.000967
	E_t	0.001173	0.001173	0.001173	0.001173	0.001176	0.001208	0.001255

trend generally holds good for all other states as well. Hence, at low- η region, CHO behaves like PISB. Now, panels (a), (b) and (c) of Fig. 1 delineate the variation of $R_{r'}^\alpha$, $R_{p'}^\beta$ and $R_t^{(\alpha,\beta)}$ respectively against η for five lowest states of a CHO corresponding to $l = 0$ to 4. Panel (a) shows that, $R_{r'}^\alpha$ falls off with rise of η implying greater localization at larger η . Interestingly at $\eta \rightarrow 0$ $R_{r'}^\alpha$ obeys the trend $R_{r'}^\alpha(1s) > R_{r'}^\alpha(1g) > R_{r'}^\alpha(1f) > R_{r'}^\alpha(1d) > R_{r'}^\alpha(1p)$. But, at large η region this trend modifies to $R_{r'}^\alpha(1g) > R_{r'}^\alpha(1f) > R_{r'}^\alpha(1d) > R_{r'}^\alpha(1p) > R_{r'}^\alpha(1s)$. Panel (b) suggests that, $R_{p'}^\beta$ accelerates with growth of η . Finally, panel (c) depicts that, $R_t^{(\alpha,\beta)}$ for $1s$ state falls off with η but for *non-zero* l states it enhances with increment of η . We also note that, at a fixed n_r both $R_{p'}^\beta$ and $R_t^{(\alpha,\beta)}$ increase with increase in quantum number l .

Now we move on to S in Table II, where $S_{r'}$, $S_{p'}$ and S_t are probed for $1s$, $1p$, $1d$ states of PISB (3rd column) and CHO (at same particular set of η as in Table I). Like R, $S_{r'}$ progresses and $S_{p'}$ diminishes with growth in η . For $l = 0$ states S_t decreases with η , while, for $l \neq 0$

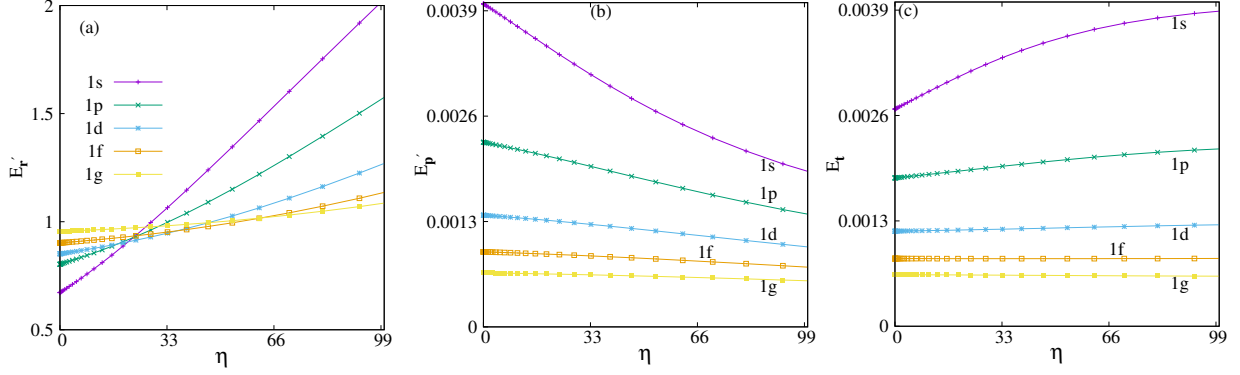


FIG. 3: Plots of E_r , E_p , E_t against η for first five circular states of CHO in panels (a), (b), (c) respectively. See text for details.

cases it mounts up. At $\eta \rightarrow 0$ region, like R, S in CHO also provides equivalent results to that of PISB. In order to gain further insight, Fig. 2 portrays $S_{r'}$, $S_{p'}$ and S_t in left (a), middle (b) and right (c) panels, for lowest five $l(0-4)$ as a function of η . But unlike $R_t^{(\alpha,\beta)}$, S_t for all these states lessen with increment in η . On the contrary, as observed in R, S's in r space at $\eta \rightarrow 0$ obeys the same order, *viz.*, $S_{r'}(1s) > S_{r'}(1g) > S_{r'}(1f) > S_{r'}(1d) > S_{r'}(1p)$. As usual at $\eta \rightarrow \infty$ this trend modifies to $S_{r'}(1g) > S_{r'}(1f) > S_{r'}(1d) > S_{r'}(1p) > S_{r'}(1s)$. Here again analogous to $R_{p'}^\beta$ and $R_t^{(\alpha,\beta)}$, both $S_{p'}$ and S_t advance with increase in l .

Now we discuss E in Table III, by providing $E_{r'}$, $E_{p'}$ and E_t of $1s, 1p, 1d$ states of selected η values used in Table I and II. Akin to R and S, E at $\eta \rightarrow 0$ delivers coequal result to that of PISB. But in other context, E shows complete reverse trends to what we have seen in R and S. $E_{r'}$, E_t advance and $E_{p'}$ reduces with improvement in η . Above changes in $E_{r'}$, $E_{p'}$ and E_t are graphically displayed in Figure 3, in left (a), middle (b), right (c) panels for first five circular states ($n_r = 1$ and $l = 0-4$). Here one can see that, $E_{r'}$, E_t decrease and $E_{p'}$ increases with progress of η . As η approaches zero, $E_{r'}$ obeys the trend $E_{r'}(1g) > E_{r'}(1f) > E_{r'}(1d) > E_{r'}(1p) > E_{r'}(1s)$ which gets reversed to $E_{r'}(1s) > E_{r'}(1p) > E_{r'}(1d) > E_{r'}(1f) > E_{r'}(1g)$ at opposite η limit. Whereas, at a fixed n_r , both $E_{p'}$ and E_t collapse with rise in l .

Upto now, we were concerned about the effect of change of η in CHO. This investigation clearly reveals that, at $\eta \rightarrow 0$ CHO behaves alike to PISB. But, since, $\eta \propto \omega r_c^4$, these results includes combined effect of both η and r_c . In order to get a complete picture of confinement effect, these two factors need to be segregated. Now, we concentrate on analysing all these quantities with respect to r_c . Later we also examine the behaviour of IE with change of n_r

TABLE IV: R_r^α, R_p^β and $R_t^{\alpha,\beta}$ values for $1s, 2s, 1p, 2p, 1d, 2d$ orbitals in CHO at eight selected r_c values. See text for detail.

r_c	R_r^α	R_p^β	$R_t^{\alpha,\beta}$	r_c	R_r^α	R_p^β	$R_t^{\alpha,\beta}$
1s				2s			
0.1	-6.0366917844	12.247171978	6.2104801936	0.1	-6.0653334752	14.2515610845	8.186227609
0.2	-3.9572613535	10.167740386	6.2104790325	0.2	-3.9858896952	12.1721134683	8.186223773
0.5	-1.2088403559	7.41927227	6.21043191	0.5	-1.2369267194	9.422993967	8.18606724
1.0	0.86363060146	5.3460818801	6.2097124816	1.0	0.8438971150	7.339578635	8.18347575
2.0	2.82653053607	3.3731259092	6.1996564453	2.0	2.9410466015	5.15805124	8.09909784
5.0	3.63268067673	2.5410652239	6.1737459006	5.0	4.5764993107	2.6162033	7.1927026
8.0	3.632690916310	2.5410540440	6.1737449603	8.0	4.5767695172	2.61482528	7.191594797
∞	3.6326909163101	2.5410540440	6.1737449603	∞	4.5767695172	2.614825285	7.1915948022
1p				2p			
0.1	-6.1671363542	12.806502114	6.6393657598	0.1	-6.29011971	14.178463580	7.88834387
0.2	-4.0876997330	10.727065993	6.63936626	0.2	-4.21067738	12.09902562	7.88834824
0.5	-1.3390273792	7.978413948	6.639386568	0.5	-1.46177311	9.35029899	7.88852588
1.0	0.7373200936	5.902381495	6.639701588	1.0	0.618160513	7.273091288	7.891251801
2.0	2.7629313961	3.882363728	6.6452951241	2.0	2.704922872	5.226357439	7.931280311
5.0	3.8830108378	2.834907070	6.7179179078	5.0	4.575880956	2.9828085	7.558689456
8.0	3.883056660633	2.8349473768	6.7180040374	8.0	4.57683522	2.982008644	7.558843864
∞	3.883056660633	2.8349473768	6.7180040374	∞	4.57683522	2.982008644	7.558843864
1d				2d			
0.1	-6.1181191683	13.2289542792	7.1108351109	0.1	-6.2478841627	14.295117242	8.0472330793
0.2	-4.0386800101	11.1495160962	7.1108360861	0.2	-4.1684423307	12.21567885	8.047236519
0.5	-1.2899046230	8.400780312	7.110875689	0.5	-1.4195583633	9.466934869	8.047376505
1.0	0.7880364400	6.323450880	7.11148732	1.0	0.6600654534	7.389472850	8.049538303
2.0	2.8408556597	4.2808923084	7.1217479681	2.0	2.7424775770	5.34296287	8.08544044
5.0	4.2284239258	3.0468595	7.2752834258	5.0	4.8017869530	3.2330682	8.0348551
8.0	4.22859084294	3.047026004	7.2756168469	8.0	4.804603250039670	3.2306644880	8.035267738
∞	4.22859084294	3.047026004	7.2756168469	∞	4.804603250039670	3.2306644880	8.035267738

at certain selected r_c values namely 0.1, 2.5, 3, 5, ∞ . In both the cases we will keep ω fixed at one. Now, onwards we will use unprimed variables in IE suffixes.

We will now study the variation of all these information measures with change of r_c . It is expected that, a progressively larger r_c should lead to a delocalization of the system in such a fashion that, at $r_c \rightarrow \infty$ it should come out to IHO. Whereas, when $r_c \rightarrow 0$ impact of confinement is maximum. Here, calculation are pursued by choosing r_c values starting from 0.1 to 10. This, parametric increase in r_c elicit the system from extremely confined environment to free situation.

To begin with, Table IV impresses calculated R_r^α, R_p^β and $R_t^{(\alpha,\beta)}$ for first two s, p and d

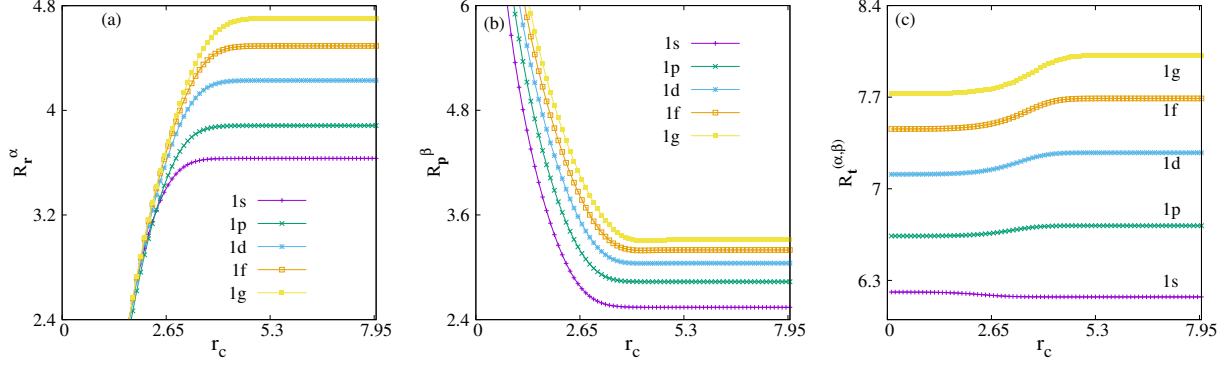


FIG. 4: Plots of R_r^α , R_p^β , $R_t^{(\alpha,\beta)}$ against r_c for first five circular states of CHO in panels (a), (b), (c) respectively. See text for details.

orbitals ($n_r = 1, 2$) of CHO at a selected set of eight r_c values. In this and all following tables of CHO, IEs are furnished for these six states considering same set of r_c values. R_r^α 's starting from particular negative values at very low r_c , continuously advance, finally merges to the respective IHO behaviour. In contrast, R_p^β 's in for all these six states generally tend to diminish with r_c , again converging to IHO in the end. Consequently, the $R_t^{(\alpha,\beta)}$ for $1s$ and $2s$ states deplete with r_c to reach the borderline values. However, for $l \neq 0$ states it enhances with r_c to attain the limiting values. At very low r_c values $n_r = 1$ states have higher R_r^α values with respect to their $n_r = 2$ counterparts. But, at moderate r_c region this trend gets reverses. Moreover, this crossover regions switch to higher r_c values with rise of l quantum number. This, observation infers that, the effect of confinement is more on higher n_r states. There are no such crossover in R_p^β and $R_t^{(\alpha,\beta)}$ in any of these states. Unfortunately no literature is available to make direct comparison with these computed values. Above observation is graphically depicted in Figure 4, where in segments (a)-(c), R_r^α , R_p^β and $R_t^{(\alpha,\beta)}$ of first five circular states with respected to r_c are portrayed. Panel (a) imprints that, for all of them, R_r^α 's quite steadily progress with r_c and finally convene to IHO. Similarly, from panel (b) it is clear that, R_p^β shows opposite pattern with r_c , before reaching IHO-limit. Panel (c) reveals that, for $l = 0$ state $R_t^{(\alpha,\beta)}$ decreases with r_c . But, for $l \neq 0$ states reverse trend is observed. However, for all these five states $R_t^{(\alpha,\beta)}$'s finally converge to their respective IHO values.

To gain further knowledge, Figure 5 delineates R_r^α , R_p^β and $R_t^{(\alpha,\beta)}$, in left (a), middle (b), right (c) panels, for lowest five node-less states as a function of n_r (maximum of 9). Five different r_c 's are taken, that is, 0.1, 2.5, 3, 5, ∞ in segments (A)-(E) from bottom to top. At

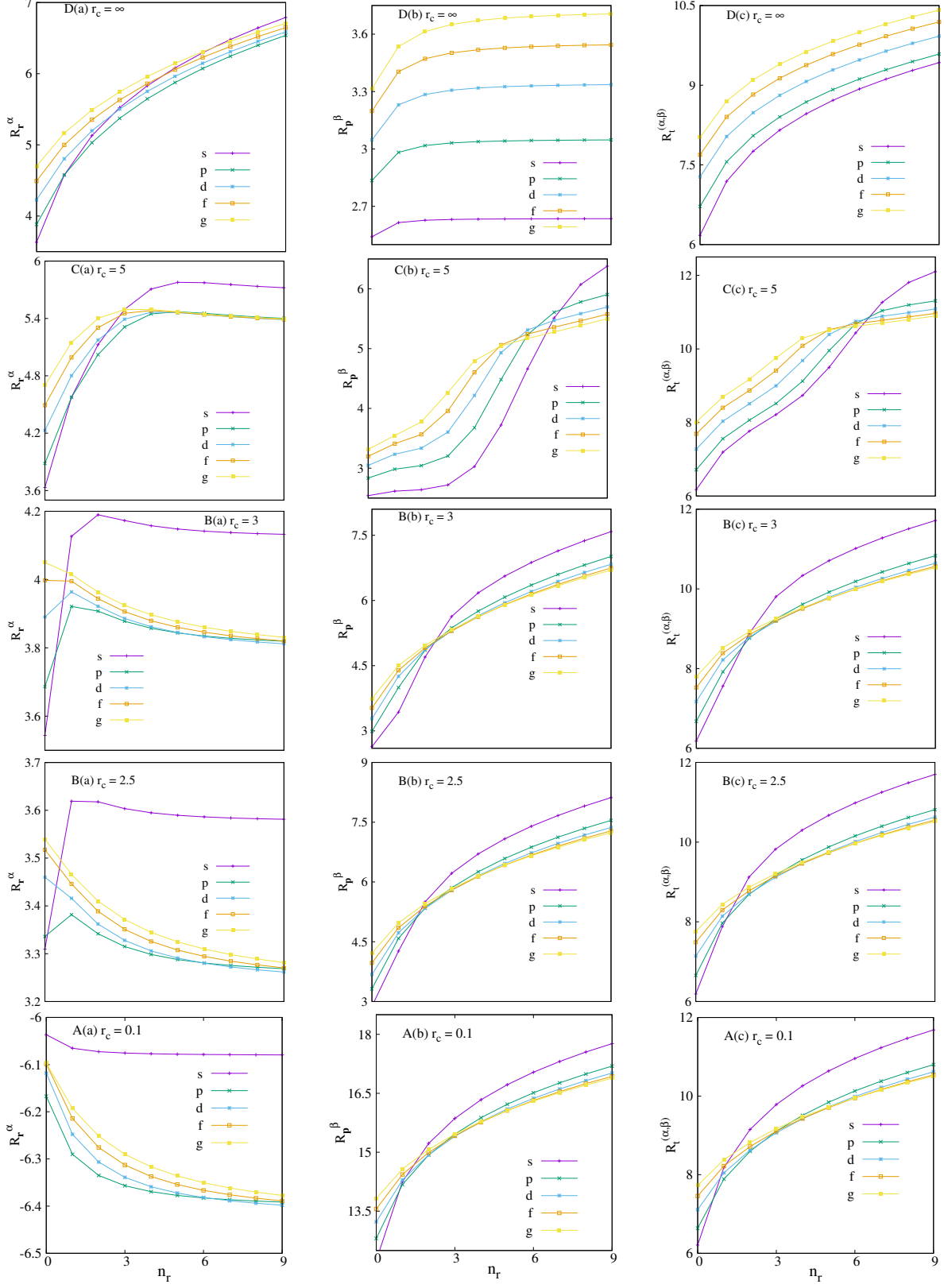


FIG. 5: Plot of R_r^α (a), R_p^β (b) and $R_t^{(\alpha,\beta)}$ (c) versus n_r (at $\omega = 1$) for s, p, d, f, g states at five particular r_c 's of CHO, namely, 0.1, 2.5, 3, 5, ∞ in panels (A)-(E). $R_t^{(\alpha,\beta)}$'s for all these states obey the lower bound given in Eq. (19). For more details, consult text.

$r_c = 0.1$, for all l , $R_{\mathbf{r}}^\alpha$'s gradually falls off with n_r . Albeit, it provides highest values for $l = 0$ states. But, for *non-zero* l states, it grows up with rise in l values. Hence, it can be concluded that, effect of confinement is maximum for $l = 1$ states and minimum for $l = 0$ states. However, higher n_r states experience the confinement in greater extent. Both, $R_{\mathbf{p}}^\beta$ (a) and $R_t^{(\alpha,\beta)}$ show reverse trend. At, low n_r values both these quantities obey the trend $1g > 1f > 1d > 1p > 1s$. This, pattern gets inversed ($1s > 1p > 1d > 1f > 1g$) at higher n_r . These results clearly indicates that, At lower r_c region quantum effect gets amplified as information content decreases, whereas, total information (uncertainty) increases with n_r . First column (a), interesting show appearance of maximum in $R_{\mathbf{r}}^\alpha$ with regular advancement of r_c . Position of these maxima gets right shifted as r_c intensifies. Apparently, there exists an interplay between two conjugate aspects: (i) radial confinement (localisation) and (ii) accumulation of nodes with n_r (delocalisation). As, r_c progresses, delocalisation predominates for lower n_r states. Hence., with continuous relaxation in confinement, states having higher n_r value gets delocalised. At, $r_c \rightarrow \infty$, second effect prevails, system behaves as IHO. In second and third columns, one can sees that, both $R_{\mathbf{p}}^\beta$ and $R_t^{(\alpha,\beta)}$ always accelerate with n_r . At $r_c \rightarrow \infty$, these two quantities approaches to respective IHO-limits.

Now, we move to S in Table V, where, $S_{\mathbf{r}}, S_{\mathbf{p}}$ and S_t are presented for $1s, 2s, 1p, 2p, 1d, 2d$ states of CHO at same set of r_c as in Table IV. Once again, no reference work exists for these, which could be compared. Like $R_{\mathbf{r}}^\alpha$, $S_{\mathbf{r}}$ also yield (-)ve values for all these six states at very low r_c and then continuously progress, until reaching the borderline IHO values. However, like $R_{\mathbf{p}}^\beta$, $S_{\mathbf{p}}$ offers an opposite nature of $S_{\mathbf{r}}$, ($R_{\mathbf{r}}^\alpha$); from an initial (+)ve, consistently reduces to reach IHO. S_t 's for both $1s, 1p$ states decrease to reach IHO values. But, for $1d$ state it falls off, reaches a minimum and finally converges to IHO.

Next, Figure 6 indicates behavioral patterns of $S_{\mathbf{r}}, S_{\mathbf{p}}, S_t$ with r_c in segments (a)-(c), for same five states Figure 6. It is important to point out that, panels (a),(b),(c) of both Figures 4 and 6 deliver similar style. For all these states $S_{\mathbf{r}}$'s mount up with r_c and finally convene to corresponding r -space IHO, while $S_{\mathbf{p}}$'s decrement before attaining that. Panel (c) shows that, for $1s, 1p$ states S_t 's decrease with r_c and finally merge to IHO, while for $1d, 1f, 1g$ states, there appears a minimum before reaching the limiting IHO values.

In Figure 7, $S_{\mathbf{r}}$ (a), $S_{\mathbf{p}}$ (b), S_t (c) of $l = 0 - 4$ states are plotted against n_r at same five r_c of Figure 5, in panels (A)-(E) from bottom to top. Again, the graphs in Figure 7 imprint

TABLE V: S_r, S_p and S_t values for $1s, 2s, 1p, 2p, 1d, 2d$ orbitals in CHO at eight selected r_c values. See text for detail.

r_c	S_r	S_p	S_t	r_c	S_r	S_p	S_t
1s				2s			
0.1	-6.232173222	12.8494	6.6172	0.1	-6.4460987687	14.6389	8.1928
0.2	-4.152747179	10.7700	6.6172	0.2	-4.3666534417	12.5595	8.1928
0.5	-1.404504328	8.0214	6.6168	0.5	-1.6176276192	9.8106	8.1929
1.0	0.6652222004	5.9458	6.6110	1.0	0.4641636149	7.731	8.195
2.0	2.5846810393	3.9492	6.5338	2.0	2.5761673628	5.654	8.230
5.0	3.2170947394	3.21709491	6.4341896494	5.0	4.1507295460	4.1510	8.3017
8.0	3.2170948239	3.217094821	6.4341896449	8.0	4.1507455435	4.15074	8.30148
∞	3.2170948239	3.2170948239	6.4341896478	∞	4.1507455435	4.1507455435	8.301491087
1p				2p			
0.1	-6.38738206	13.417	7.029	0.1	-6.651966568	14.7283	8.0763
0.2	-4.30794705	11.338	7.030	0.2	-4.572523919	12.6489	8.0763
0.5	-1.55934019	8.5894	7.0300	0.5	-1.823606736	9.9000	8.0763
1.0	0.51599338	6.5114	7.0273	1.0	0.256528223	7.82132	8.07784
2.0	2.5241140868	4.4663	6.9904	2.0	2.346915762	5.753	8.099
5.0	3.4874566574	3.487448	6.974904	5.0	4.1477548396	4.1483	8.2960
8.0	3.4874576660	3.487457668	6.974915334	8.0	4.14786196159	4.147863	8.295724
∞	3.4874576660	3.4874576660	6.974915332	∞	4.14786196159	4.14786196159	8.2957239232
1d				2d			
0.1	-6.3553068427	14.0035	7.6481	0.1	-6.5939939435	15.0676	8.4736
0.2	-4.2758683878	11.9241	7.6482	0.2	-4.5145520348	12.988	8.473
0.5	-1.527121568	9.1753	7.6481	0.5	-1.7656649279	10.2393	8.4736
1.0	0.5503764295	7.0964	7.6467	1.0	0.3140078818	8.1605	8.4745
2.0	2.5952812036	5.0319	7.6271	2.0	2.3974788669	6.091	8.488
5.0	3.8426303929	3.84259239	7.68522278	5.0	4.3885945973	4.3909	8.7794
8.0	3.8426381378	3.84263813	7.68527626	8.0	4.389113529281	4.38910	8.77821
∞	3.8426381378	3.8426381378	7.6852762756	∞	4.389113529281	4.389113529281	8.7782270586

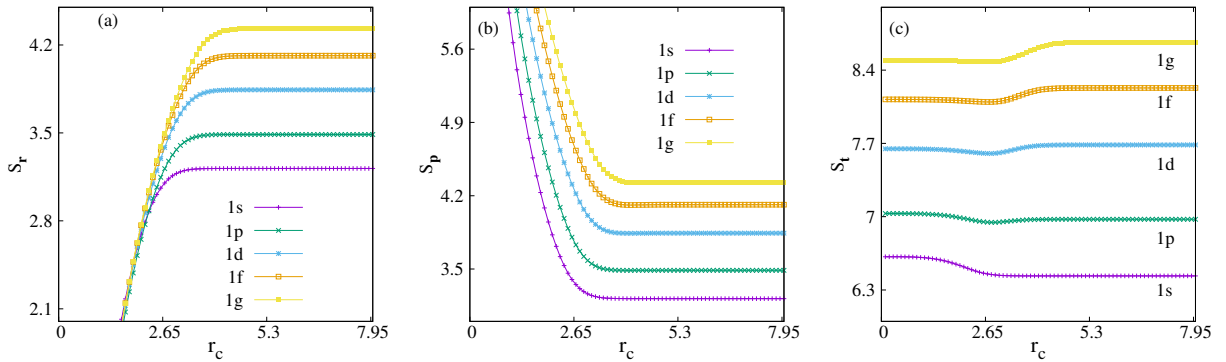


FIG. 6: Plots of S_r, S_p, S_t against r_c for first five circular states of CHO in panels (a), (b), (c) respectively. See text for details.

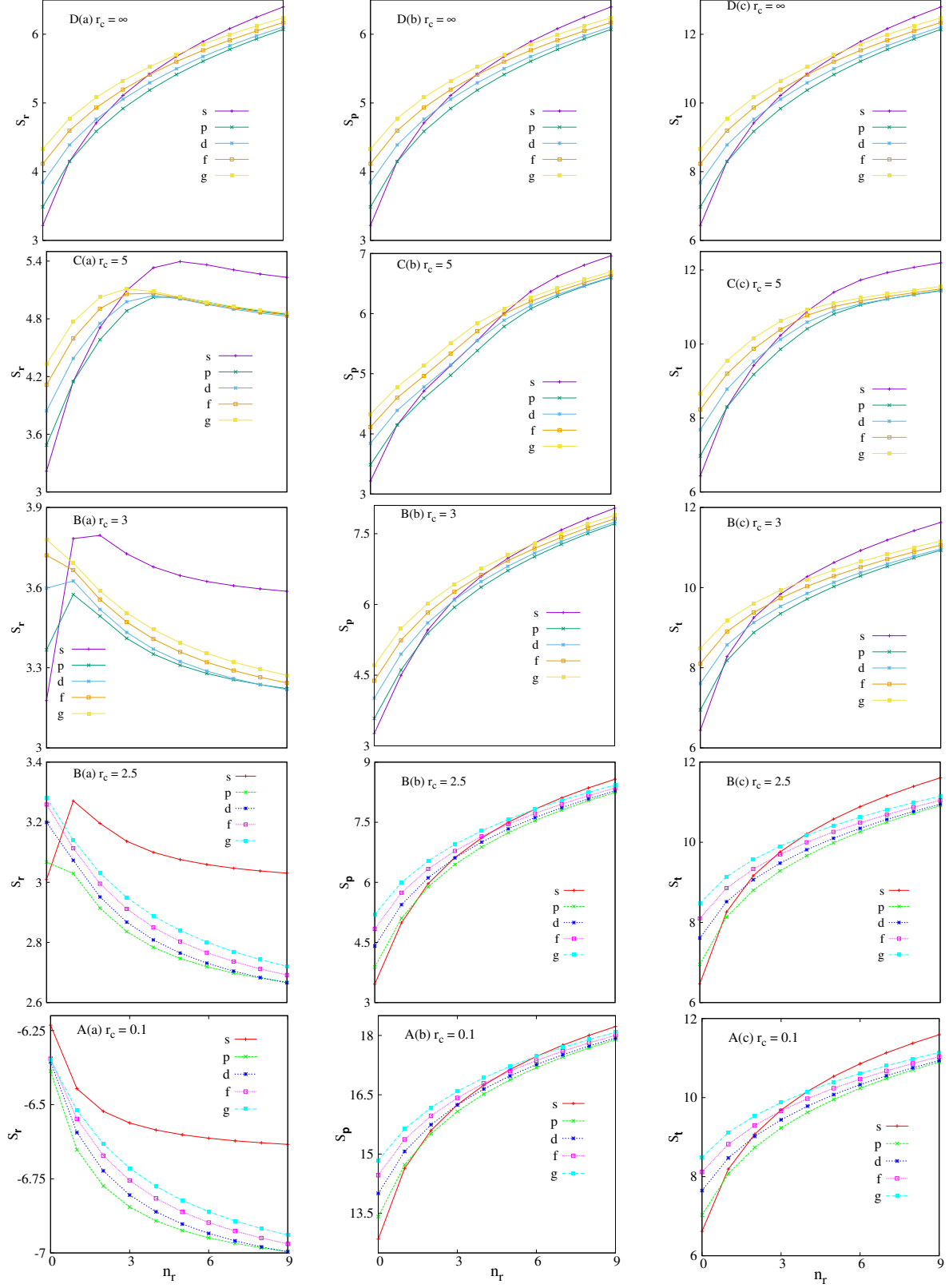


FIG. 7: Plot of S_r (a), S_p (b) and S_t (c) versus n_r (at $\omega = 1$) for s, p, d, f, g states at five particular r_c 's of CHO, namely, 0.1, 2.5, 3, 5, ∞ in panels (A)-(E). S_t 's for all these states obey the lower bound given in Eq. (19). For more details, consult text.

TABLE VI: E_r, E_p and E_t values for $1s, 2s, 1p, 2p, 1d, 2d$ orbitals in CHO at eight selected r_c values. See text for detail.

r_c	E_r	E_p	E_t	r_c	E_r	E_p	E_t
$1s$				$2s$			
0.1	672.0719164	0.0000039863	0.0026791	0.1	1453.1909702895	0.00000057	0.00082825
0.2	84.01080088	0.0000318904	0.0026791	0.2	181.6485572148	0.000004559	0.000828257
0.5	5.3814002356	0.0004980894	0.002680418	0.5	11.6246913489	0.000071246	0.000828213
1.0	0.6818097823	0.0039601229	0.0027000505	1.0	1.4515093698	0.0005701466	0.0008275732
2.0	0.1056762183	0.0284605182	0.0030075999	2.0	0.1784022679	0.004660181	0.000831386
5.0	0.0634936361	0.0634934018	0.004031427	5.0	0.0406758398	0.0406482969	0.0016534036
8.0	0.0634936347	0.0634936349	0.0040314417	8.0	0.040670749	0.0406756097	0.0016543075
∞	0.0634936347	0.0634936347	0.0040314416	∞	0.0406756097	0.0406756097	0.0016545052
$1p$				$2p$			
0.1	803.22700816	0.0000022775	0.0018293897	0.1	1454.974575234	0.0000005896	0.000857877
0.2	100.40423515	0.0000182203	0.0018294011	0.2	181.8717931823	0.000004717	0.0008578847
0.5	6.4281046025	0.0002846331	0.0018296512	0.5	11.6397197874	0.0000736934	0.0008577713
1.0	0.8078468658	0.0022696156	0.0018335018	1.0	1.454810759	0.0005883981	0.0008560079
2.0	0.1107979053	0.0171292823	0.0018978886	2.0	0.1813047648	0.004569953	0.0008285543
5.0	0.0476202385	0.0476216277	0.0022677533	5.0	0.0324128865	0.0323758305	0.0010493941
8.0	0.047620224	0.0476202241	0.0022676857	8.0	0.032411515	0.0324115148	0.0010505063
∞	0.047620224	0.047620224	0.0022676857	∞	0.032411515	0.032411515	0.0010505063
$1d$				$2d$			
0.1	851.25726418	0.000001378	0.0011730159	0.1	1368.86082394	0.0000004746	0.0006496614
0.2	106.40757650	0.0000110238	0.0011730187	0.2	171.107627763	0.0000037968	0.0006496761
0.5	6.8111728555	0.0001722254	0.0011730568	0.5	10.9509523492	0.0000593197	0.0006496078
1.0	0.8535077417	0.0013750845	0.0011736453	1.0	1.3689869817	0.0004737266	0.0006485256
2.0	0.1114898571	0.0106198478	0.0011840053	2.0	0.1712007721	0.0036813808	0.0006302552
5.0	0.0357152613	0.0357193674	0.0012757265	5.0	0.0249812774	0.0249259554	0.0006226822
8.0	0.0357151695	0.0357151695	0.0012755733	8.0	0.0249755634	0.0249755633	0.0006237788
∞	0.0357151695	0.0357151695	0.0012755733	∞	0.0249755634	0.0249755634	0.0006237788

analogous shape and propensity to that of Figure 5. Thus in coherence with R_r^α at $r_c = 0.1$, for five l , S_r gets lowered in A(a), while S_p 's and S_t 's improve with n_r in A(b) and A(c), respectively. This reinforces our previous epilogue (as in R in Figure 4) that, at very low r_c , effect of confinement is more prevalent in high-lying states, signifying a intensification of quantum nature in such circumstances. As usual, like R_r^α here also, the first column ((a)) of Figure 7 render the appearance of maximum in S_r plots with gradual growth of r_c . Their position gets shifted to right as r_c improves. This observation indicates that, at $r_c \rightarrow \infty$ system behaves like IHO.

At this stage we move on to explore the last measure of this study, that is, E in Table

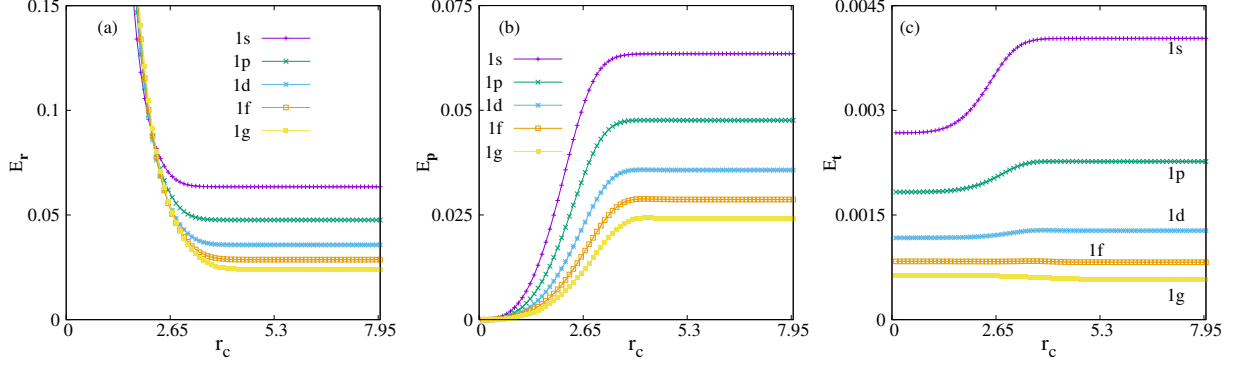


FIG. 8: Plots of E_r , E_p , E_t against r_c for first five circular states of CHO in panels (a), (b), (c) respectively. See text for details.

VI. A cross-section of E_r , E_p and E_t for $1s, 2s, 1p, 2p, 1d, 2d$ states of CHO (same set of r_c values used for previous measures) is offered. One notices that, E_r decreases (as opposed to R_r^α, S_r) while E_p accelerates (as opposed to R_p^β, S_p) with progress in r_c . However, behaviour of E_t with r_c varies from state to state. For $1s, 1p, 1d$ states it advances with r_c . But, for $2s$ and $2p$ states it passes through a minimum and in case of $2d$ state it always falls off with increase in boundary.

These changes in E_r, E_p and E_t with r_c are graphically displayed in Figure 8, in left (a), middle (b) and right (c) panels for first five circular states. One notices that, E_t for $1s, 1p, 1d$ states increases with r_c , while for $1f, 1g$ states it decreases. Interestingly, at large r_c , both E_r and E_p decrease with increase in l .

In Figure 9, E_r, E_p and E_t are portrayed (in columns (a),(b),(c)) for $l = 0 - 4$ states as functions of n_r at five different r_c values (in segments A-E). At the lowest r_c considered, E_r progresses with n_r . However, the first column (a) suggests that, a minimum appears in E_r graphs as r_c is extended. Also the positions of these minima gets right shifted with increment in r_c . On the contrary, for all concern r_c values, both E_p, E_t diminish with n_r .

IV. FUTURE AND OUTLOOK

Information theoretic measures like R, S, E are pursued for CHO in both r, p spaces, along with their composite measures. At first, in order to explore the composite effects of ω and r_c , the Hamiltonian is transformed into a dimensionless form. This established that, CHO behaves as an interim model between the PISB and IHO. Later, the role of

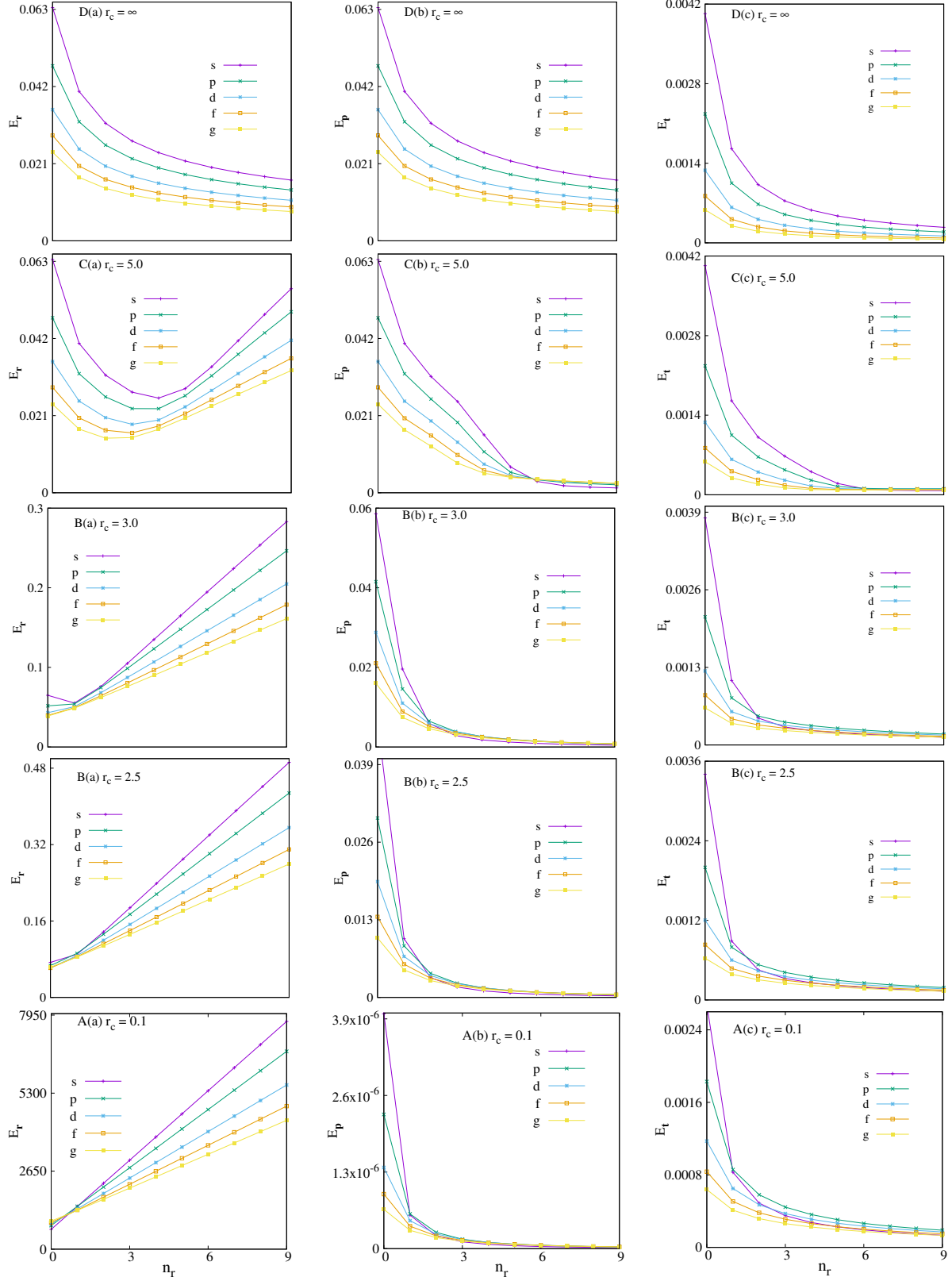


FIG. 9: Plot of E_r (a), E_p (a) and E_t (c) versus n_r (at $\omega = 1$) for s, p, d, f, g states at five particular r_c 's of CHO, namely, 0.1, 2.5, 3, 5, ∞ in panels (A)-(E). S_t 's for all these states obey the lower bound given in Eq. (19). For more details, consult text.

r_c on these measures were investigated keeping ω fixed at 1. Amongst several interesting features, one notices that, at very low r_c , R_r^α , S_r fall and E_r grows as n_r advances, which is in sharp contrast to that found in IHO. Furthermore, r_c and η produce opposite effects on IE measures. The effect of nonzero m and a penetrable cavity on these measures may lead to some other interesting features, which may be pursued later.

V. ACKNOWLEDGEMENT

Financial support from DST SERB, New Delhi, India (sanction order: EMR/2014/000838) is gratefully acknowledged. NM thanks DST SERB, New Delhi, India, for a National-post-doctoral fellowship (sanction order: PDF/2016/000014/CS).

-
- [1] A. Michels, J. de Boer and A. Bijl, *Physica* **4**, 981 (1937).
 - [2] J. R. Sabin, E. Brändas and S. A. Cruz (Eds.), *The Theory of Confined Quantum Systems*, Parts I and II, *Advances in Quantum Chemistry*, Vols. 57 and 58 (Academic Press, 2009).
 - [3] K. D. Sen (Ed.), *Electronic Structure of Quantum Confined Atoms and Molecules*, (Springer, Switzerland, 2014).
 - [4] A. Sarsa and C. Le Sech, *J. Chem. Theory Comput.* **7**, 2786 (2011).
 - [5] C. Le Sech and A. Banerjee, *J. Phys. B* **44**, 105003 (2011).
 - [6] J. Katriel and H. E. Montgomery Jr., *J. Chem. Phys.* **137**, 114109 (2012).
 - [7] R. Cabrera-Trujillo and S. A. Cruz, *Phys. Rev. A* **87**, 012502 (2013).
 - [8] H. Pang, W-S. Dai and M. Xie, *J. Phys. A* **44**, 365001 (2011).
 - [9] N. Aquino, *J. Phys. A* **30**, 2403 (1997).
 - [10] N. Sobrino-Coll, D. Puertas-Centeno, I. V. Toranzo and J. S. Dehesa, *J. Stat. Mech.* **8**, 083102 (2017).
 - [11] G. Campoy, N. Aquino and V. D. granados, *J. Phys. A* **35**, 4903 (2002).
 - [12] H. E. Montgomery Jr., N. A. Aquino and K. D. Sen, *Int. J. Quant. Chem.* **107**, 798, (2007)
 - [13] A. K. Roy, *Mod. Phys. Lett. A* **29**, 1450104 (2014); *ibid.*, **30**, 1550176 (2015).
 - [14] A. Ghosal, N. Mukherjee and A. K. Roy, *Ann. Phys. (Berlin)* **528**, 796, (2016).
 - [15] H. E. Montgomery Jr., N. A. Aquino and K. D. Sen, *Int. J. Quant. Chem.* **107**, 798 (2007).

- [16] S. Goldman and C. Joslin, J. Phys. Chem. **96**, 6021 (1992).
- [17] N. Aquino A., Int. J. Quant. Chem. **54**, 107 (1995).
- [18] J. Garza, R. Vargas and A. Vela, Phys. Rev. E **58**, 3949 (1998).
- [19] C. Laughlin, B. L. Burrows and M. Cohen, J. Phys. B **35**, 701 (2002).
- [20] B. L. Burrows and M. Cohen, Int. J. Quant. Chem. **106**, 478 (2006).
- [21] N. Aquino, G. Campoy and H. E. Montgomery Jr., Int. J. Quant. Chem. **107**, 1548 (2007).
- [22] D. Baye and K. D. Sen, Phys. Rev. E **78**, 026701 (2008).
- [23] H. Ciftci, R. L. Hall and N. Saad, Int. J. Quant. Chem. **109**, 931 (2009).
- [24] A. K. Roy, Int. J. Quant. Chem. **115**, 937 (2015).
- [25] D. Puertas-Centeno, N. M. Temme, I. V. Toranzo and J. S. Dehesa, J. Math. Phys. **58**, 103302 (2017).
- [26] H. G. Laguna and R. P. Sagar, Ann. Phys. (Berlin) **526**, 555, (2014).
- [27] N. Mukherjee and A. K. Roy, Int. J. Quant. Chem. e25596 (2018).
- [28] N. Mukherjee, S. Majumdar and A. K. Roy, Chem. Phys. Lett. **691**, 449 (2018).
- [29] S. Majumdar, N. Mukherjee and A. K. Roy, Chem. Phys. Lett. **687**, 322 (2017).
- [30] N. Mukherjee and A. K. Roy, Euro. Phys. J. D (in press).
- [31] S. H. Patil, K. D. Sen, N. A. Watson and H. E. Montgomery Jr., J. Phys. B **40**, 2147 (2007).
- [32] W. Zawadzki, Semicond. Sci. Technol. **2**, 550, (1987).
- [33] M. Büttiker, Phys. Rev. B, **38**, 0375 (1988).
- [34] I. Varga and J. Pipek, Phys. Rev. E **68**, 026202 (2003).
- [35] R. Renner, N. Gisin and B. Kraus, Phys. Rev. A **72**, 012332 (2005).
- [36] P. Lévy, S. Negy and J. Pipek, Phys. Rev. A **72**, 022302 (2005).
- [37] F. Verstraete and J. I. Cirac, Phys. Rev. B **73**, 094423 (2006).
- [38] A. Bialas, W. Czyz and K. Zalewski, Phys. Rev. C **73**, 034912 (2006).
- [39] L. L. Salcedo, J. Math. Phys. **50**, 012106 (2009).
- [40] S.-B. Liu, C.-Y. Rong, Z.-M. Wu and T. Lu, Acta. Phys.-Chim. Sin. **31**, 2057 (2015).
- [41] K. D. Sen (Ed.), *Statistical Complexity: Applications in Electronic Structure*, (Springer, 2012).
- [42] I. Bialynicki-Birula, Phys. Rev. A **74**, 052101 (2006).
- [43] O. Onicescu, C. R. Acad. Sci. Paris A **263**, 25 (1966).
- [44] G.-H. Sun, M. A. Aoki and S.-H. Dong, Chin. Phys. B **22**, 050302 (2013).
- [45] G.-H. Sun, S.-H. Dong and N. Saad, Ann. Phys. (Berlin) **525**, 934 (2013).

- [46] W. A. Yahya, K. J. Oyewumi and K. D. Sen, *Int. J. Quant. Chem.* **115**, 1543 (2015).
- [47] S. Dong, G.-H. Sun, S.-H. Dong and J. P. Draayer, *Phys. Lett. A* **378**, 124 (2014).
- [48] R. Valencia-Torres, G.-H. Sun and S.-H. Dong, *Phys. Scr.* **90**, 035205 (2015).
- [49] G.-H. Sun, P. Duan, C.-N. Oscar and S.-H. Dong, *Chin. Phys. B* **24**, 100303 (2015).
- [50] G. Yañez-Navarro, G.-H. Sun, T. Dytrych, K. D. Launey, S.-H. Dong and J. P. Draayer, *Ann. Phys.* **348**, 153 (2014).
- [51] X.-D. Song, G.-H. Sun and S.-H. Dong, *Phys. Lett. A* **379**, 1402 (2015).
- [52] G.-H. Sun, S.-H. Dong, K. D. Launey, T. Dytrych and J. P. Draayer, *Int. J. Quant. Chem.* **115**, 891 (2015).
- [53] N. Mukherjee, A. Roy and A. K. Roy, *Ann. Phys. (Berlin)* **527**, 825, (2015).
- [54] N. Mukherjee and A. K. Roy, *Ann. Phys. (Berlin)* **528**, 412, (2016).
- [55] R. G. González-Férez and J. S. Dehesa, *Phys. Rev. Lett.* **91**, 113001 (2003).
- [56] I. Bialynicki-Birula and J. Mycielski, *Commun. Math. Phys.* **44**, 129, (1975).
- [57] E. Romera, P. Sánchez-Moreno and J. S. Dehesa, *Chem. Phys. Lett.* **414**, 468 (2005).
- [58] A. K. Roy, A. F. Jalbout and E. I. Proynov, *J. Math. Chem.* **44**, 260 (2008).
- [59] A. K. Roy, A. F. Jalbout and E. I. Proynov, *Int. J. Quant. Chem.* **108**, 827 (2008).
- [60] A. K. Roy, *Mod. Phys. Lett. A* **29**, 1450042 (2014), *ibid.*, **29**, 1450104 (2014).